

Tunable Self-Assembly of Triazole-Linked Porphyrin–Polymer Conjugates

Derrick A. Roberts,^[a, b] Timothy W. Schmidt,^[b] Maxwell J. Crossley,^{*[b]} and Sébastien Perrier^{*[a]}

Abstract: The convergence of supramolecular chemistry and polymer science offers many powerful approaches for building functional nanostructures with well-defined dynamic behaviour. Herein we report the efficient “click” synthesis and self-assembly of AB₂- and AB₄-type multitopic porphyrin–polymer conjugates (PPCs). PPCs were prepared using the copper(I)-catalysed azide–alkyne cycloaddition (CuAAC) reaction, and consisted of linear polystyrene, poly(butyl acrylate), or poly(*tert*-butyl acrylate) arms attached to a

zinc(II) porphyrin core via triazole linkages. We exploit the presence of the triazole groups obtained from CuAAC coupling to direct the self-assembly of the PPCs into short oligomers (2–6 units in length) via intermolecular porphyrinatozinc–triazole coordination. By altering the length and grafting density of the polymer arms,

Keywords: click chemistry • cycloaddition • porphyrins • polymerization • supramolecular chemistry

we demonstrate that the association constant of the porphyrinatozinc–triazole complex can be systematically tuned over two orders of magnitude. Self-assembly of the PPCs also resulted in a 6 K increase in the glass transition temperature of the bulk material compared to a non-assembling PPC. The modular synthesis and tunable self-assembly of the triazole-linked PPCs thus represents a powerful supramolecular platform for building functional nanostructured materials.

Introduction

The recent convergence of supramolecular chemistry^[1] and controlled polymerisation techniques^[2] offers powerful tools for designing hierarchically-organised polymer architectures for nanotechnology and nanomedicine.^[3] Synthetic polymers are promising supramolecular building blocks due to their low cost, high processability and modular functionality. By incorporating small-molecule recognition units into polymer chains, it is possible to target complex and dynamic macromolecular aggregates that may eventually mimic the structure and function of biological entities,^[4] from nucleic acids and proteins up to cells and entire living organisms.

Numerous supramolecular recognition motifs have been applied to the rapidly expanding field of polymer self-assembly. Hydrogen-bonding has featured prominently,^[5] as have metal–ligand coordination^[6], π – π stacking,^[7] and host–guest inclusion complexes.^[8] Surprisingly, porphyrin-based supramolecular complexes have been largely overlooked for directing polymer self-assembly despite their rich physical properties^[9] and well-studied supramolecular chemistry.^[10]

Earlier research efforts on porphyrin–polymer conjugates have employed microphase separation and solvophobic aggregation of amphiphilic polymers for building micelles, fibrils, and nanoparticles.^[11] Well-defined porphyrin–polymer nanostructures have also been prepared by anchoring porphyrins to poly(isocyanide)^[12] and polyethylene backbones.^[13] In these systems self-assembly was due to the aggregation behaviour of the polymer chains, with the porphyrin moiety playing an unremarkable role in the self-assembly mechanism. Zimmerman and co-workers have reported the sole example of using supramolecular porphyrin chemistry to induce the self-assembly of a synthetic polymer.^[14] At present, this powerful route for building functional nanostructures remains relatively unexplored.

Herein we report an efficient “click” synthesis of AB₂- and AB₄-type multitopic porphyrin–polymer conjugates (PPCs) using the copper(I)-catalysed azide–alkyne cycloaddition (CuAAC) reaction.^[15] The PPCs consist of linear polystyrene, poly(butyl acrylate) or poly(*tert*-butyl acrylate) arms, synthesised by reversible addition–fragmentation chain transfer (RAFT) polymerisation,^[16] attached to a zinc(II) porphyrin core via triazole linkages. We exploit the presence of the triazole group obtained from CuAAC to direct the self-assembly of the PPCs into short oligomers via intermolecular porphyrinatozinc–triazole coordination. We demonstrate that the association constant of the porphyrinatozinc–triazole complex can be tuned by altering the polymer microenvironment around the porphyrin core, and switched completely to the disassembled state by introducing pyridine as a competitive ligand. In the solid state, porphyrinatozinc–triazole self-assembly caused a 6 K increase

[a] D. A. Roberts, Prof. S. Perrier
Key Centre for Polymers and Colloids, The University of Sydney
Sydney NSW 2006 (Australia)
E-mail: sebastien.perrier@sydney.edu.au

[b] D. A. Roberts, Prof. T. W. Schmidt, Prof. M. J. Crossley
School of Chemistry, The University of Sydney
Sydney NSW 2006 (Australia)
E-mail: maxwell.crossley@sydney.edu.au

Supporting information for this article is available on the WWW under <http://dx.doi.org/10.1002/chem.201301133>.

in the glass transition temperature for $(\text{PS}_{20})_2\text{-Zn}$ compared to a non-assembled control, which we attribute to coordination-induced cross-linking of the PPCs.

Results and Discussion

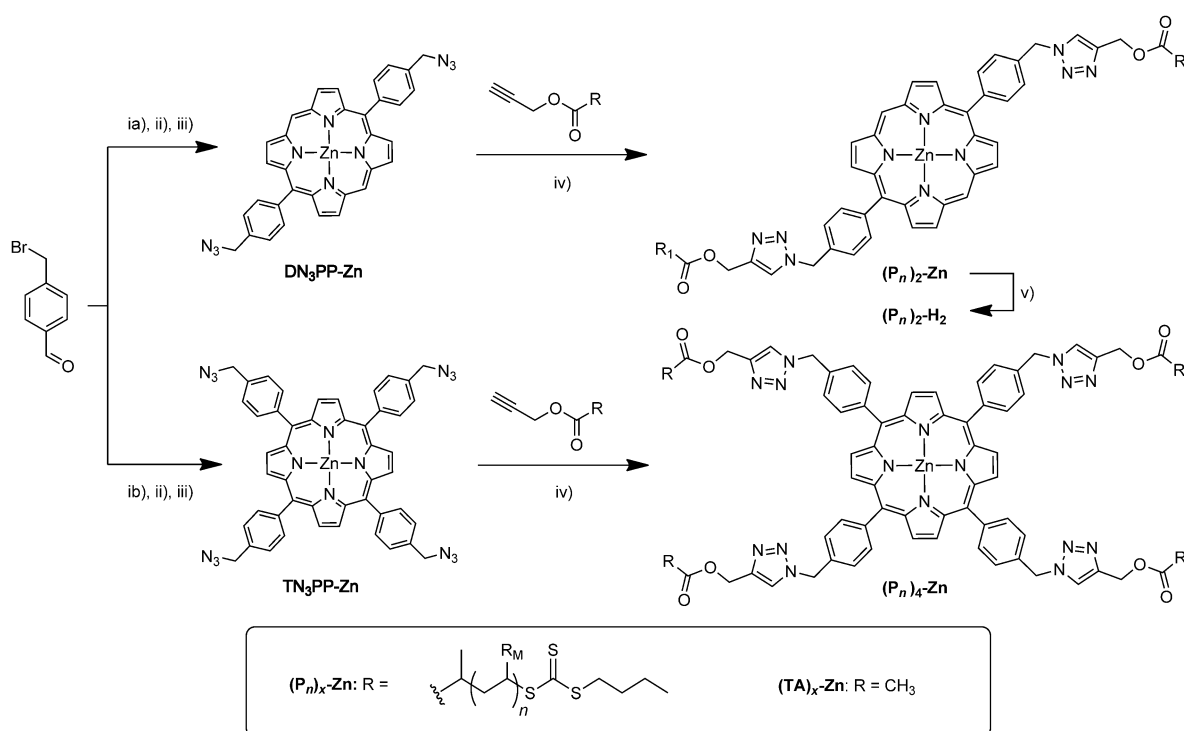
Synthesis of porphyrin-polymer conjugates: Triazole-linked PPCs were prepared from azidoporphyrin and alkyne-RAFT polymer precursors, as summarised in Scheme 1. Zinc(II) di- and tetraazidoporphyrins ($\text{DN}_3\text{PP-Zn}$ and $\text{TN}_3\text{PP-Zn}$) were obtained in 7–32% overall yield by reacting 4-(bromomethyl)benzaldehyde with either pyrrole or 2,2'-dipyrrromethane, followed by azide substitution of the resulting bromoporphyrins and subsequent zinc metallation.^[17] Alkyne-functionalised polystyrene (PS), poly(butyl acrylate) (PBA) and poly(*tert*-butyl acrylate) (PtBA) were prepared by RAFT polymerisation using an alkyne-functionalised chain transfer agent (CTA) (see Supporting Information, Section S1), which has been reported in previous work.^[18]

Alkyne-functionalised RAFT polymers were grafted to the zinc(II) azidoporphyrins using a convergent CuAAC coupling strategy previously employed by our research group (Scheme 1).^[19] Model compounds bearing triazolyl acetate arm groups, $(\text{TA})_2\text{-Zn}$ and $(\text{TA})_4\text{-Zn}$, were also prepared using the same protocol, using propargyl acetate in

place of the alkyne-polymer. These model compounds were designed to help elucidate the ^1H NMR spectra and self-assembly behaviour of the PPCs.

CuAAC coupling was performed under microwave (MW) irradiation in *N,N*-dimethylformamide (DMF) using copper(II) sulfate and sodium ascorbate to generate the copper(I) catalyst (Scheme 1). A 5–10 mol% excess of the alkyne-polymer was required to ensure that the azidoporphyrins were functionalised completely. Excess free polymer was removed by preparative size-exclusion chromatography (SEC) using Biobeads SX-1 in toluene. Chromatography was simplified by the characteristic colours of the RAFT polymer (bright yellow), two-arm PPCs (red) and four-arm PPCs (purple), which enabled direct collection of the desired bands.

Porphyrin-polymer coupling was highly efficient (87–98% conversion by ^1H NMR),^[20] yielding conjugates with the targeted number of polymer arms per porphyrin core (Table 1). Conversion was independent of the length of the grafted polymer chains, demonstrating the efficacy of the CuAAC reaction for macromolecular coupling. Average molar mass (M_n) and dispersity values (\mathcal{D}) of the PPCs were determined using analytical gel permeation chromatography (GPC) (Table 1). Measured M_n values of the two-arm conjugates agreed to within 7% of the theoretical number-average molar masses ($M_{n,\text{theor}}$). $M_{n,\text{theor}}$ values of the four-arm polystyrene conjugates underestimated the measured M_n by



Scheme 1. Synthesis of porphyrin-polymer conjugates. ia) 2,2'-dipyrrromethane, trifluoroacetic acid, CH_2Cl_2 , 2 h then 2,3-dichloro-5,6-dicyano-1,4-benzoquinone (DDQ), 10%; ib) pyrrole, trifluoroacetic acid, CH_2Cl_2 , 2 h then DDQ, 38%; ii) NaN_3 , 50 °C, THF/ H_2O 4:1, 16 h, 74–88%; iii) $\text{Zn}(\text{OAc})_2 \cdot 2\text{H}_2\text{O}$, $\text{CHCl}_3/\text{CH}_2\text{OH}$ 4:1, 1 h, 90–97%; iv) $\text{CuSO}_4 \cdot 4\text{H}_2\text{O}$, sodium ascorbate, DMF, MW irradiation (100 W, 100 °C), 25 min; v) HCl (1 M), CHCl_3 , RT. P_n denotes a polymer chain with repeating unit R_M and number-average degree of polymerisation of “ n ”; “ x ” corresponds to the number of polymer or triazolyl acetate (TA) arms attached to the porphyrin core.

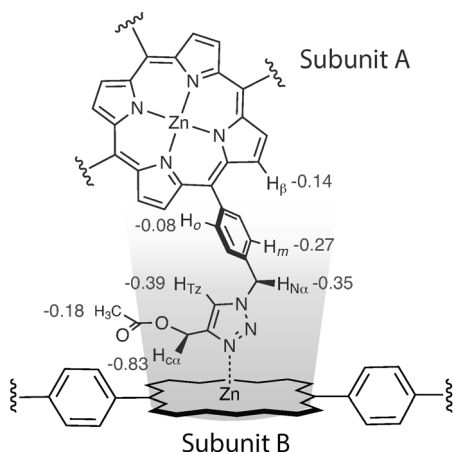


Figure 2. The $\Delta\delta$ values of protons in Subunit A correlate with their position from the centre of the porphyrin ring in Subunit B. $\Delta\delta$ (ppm) values are shown next to each proton environment. Only one of the two shielding cones of the porphyrin ring is shown.

the porphyrinatozinc and triazole subunits display intramolecular coordination.^[24] Peak broadening and the apparent D_{4h} symmetry of the porphyrin signals is consistent with ensemble averaging due to dynamic exchange between the unimeric and assembled species at a fast rate compared to the NMR timescale.^[25]

The proposed porphyrinatozinc–triazole assembly mode can be used to rationalise the change in chemical shift ($\Delta\delta$) of each proton resonance upon self-assembly of **(TA)₄-Zn**. The value of $\Delta\delta$ is taken as the difference between the assembled and unimeric chemical shifts:

$$\Delta\delta = \delta_{\text{assembled}} - \delta_{\text{unimer}} \quad (1)$$

Figure 2 shows that the $\Delta\delta$ values of protons in subunit A correlate with their positions from the centre of the porphyrin ring in subunit B. Protons situated above subunit B coincide with the shielding zone of the porphyrin's ring current field, causing diamagnetic shifting of the signals.^[26,27] The closer a proton is to the centre of the porphyrin ring, the greater the shielding effect.^[28] Values of $\Delta\delta$ are lower than those observed for other porphyrin-based host–guest complexes,^[29] which is consistent with the labile nature of the porphyrinatozinc–triazole interaction. The pattern of the $\Delta\delta$ values suggests that **(TA)₄-Zn** assembles into open acyclic structures, whereby the porphyrin rings are oriented in an approximately T-shaped geometry as shown in Figure 2. The design of the PPCs prevents the formation of closed cyclic dimers,^[30–33] which would cause a steric clash between the phenyl ring and porphyrin macrocycle on adjacent PPCs.

Two-dimensional nuclear Overhauser effect spectroscopy (NOESY) was used to probe the structure of the porphyrinatozinc–triazole complex in solution. A control ¹H–¹H NOESY experiment of **(TA)₄-Zn** in CDCl₃/[D₅]pyridine (98:2 v/v) was performed to establish the intramolecular correlations within the unimeric species (Figure 4a). The expected nearest-neighbor correlations were observed without

any anomalous long-range interactions. In particular, H_{Cα} showed only a single correlation with H_{Tz}, and there were no cross-peaks between H_β and either H_{Nα} or H_{Cα}.

When the NOESY spectrum of **(TA)₄-Zn** was recorded in neat CDCl₃, additional cross-peaks due to intermolecular correlations between H_{Cα}–H_β, H_{Cα}–H_o and H_{Nα}–H_β were observed (Figure 4b). These correlations are consistent with the intermolecular porphyrinatozinc–triazole assembly geometry illustrated in Figures 2 and 4b. Interestingly, the cross-peak between H_{Cα} and H_{Tz} observed in the control experiment was absent in the assembled state. We propose that conformational restriction within the assembled complex turns these protons away from each other, eliminating cross-relaxation.

Under the same conditions, the PPCs showed very similar self-assembly behaviour to **(TA)₄-Zn**. ¹H NMR spectra of **(PtBA₁₉)₄-Zn** have been selected as representative examples (Figure 3). ¹H NMR spectra of other assembled PPCs are shown in the Supporting Information (Section S8). In CDCl₃/[D₅]pyridine (98:2 v/v), the spectrum displays sharp signals for the porphyrin–phenylene–triazolyl spin systems, which supports a unimeric D_{4h} symmetric porphyrin core. In the absence of [D₅]pyridine, however, resonances of the porphyrin, phenyl and triazole spin systems were broadened and shifted upfield with respect to the unimer spectrum, in a similar fashion to the behaviour of **(TA)₄-Zn**. The ¹H NMR spectrum of freebase PPC **(PS₂₀)₂-H₂**, prepared by acidic demetallation of **(PS₂₀)₂-Zn** (Scheme 1), demonstrates the importance of the porphyrinatozinc moiety for PPC self-assembly: the spectrum recorded in CDCl₃ (Supporting Information, Figure S15) did not display the peak broadening and shifting observed in the zinc-PPC samples. The PPCs, therefore, do not self-assemble if the centrally-bound zinc ion is removed from the porphyrin macrocycle.

The $\Delta\delta$ values observed in the ¹H NMR spectra of the two-arm and four-arm PPCs showed similar trends to those of **(TA)₄-Zn** (Table 2). The spectral changes upon aggregation of the four-arm conjugates were nearly identical to those observed for **(TA)₄-Zn**. The two-arm conjugates also behaved similarly; however, the proton resonances of the assembled two-arm PPCs were much sharper than the analogous peaks of their four-arm counterparts, and $\Delta\delta$ values were larger, suggesting that higher grafting densities destabilise the supramolecular assemblies.

NOESY was attempted on the smallest PPC, **(PS₂₀)₂-Zn** (Figure S21). The expected intramolecular correlations were present in the control sample; however the key intermolecular correlations observed in the NOESY spectrum of assembled **(TA)₄-Zn** (i.e., H_{Cα}–H_β, etc.) were absent (Figure 4). Surprisingly, H_{Cα} did not display any cross-peaks, which suggests that NOESY is not sufficiently sensitive for detecting the through-space ¹H–¹H correlations within the PPCs. We attribute this limitation to the lability of the self-assembled oligomers, the low intensity of the porphyrin resonances compared to those of the polymer, and rapid exchange between the assembled and unimeric species. Attempts to enhance the NOE for H_{Nα} and H_{Cα} by deoxygenation of the

Table 2. Values of $\Delta\delta$ for various zinc(II) PPCs. ^1H NMR spectra recorded at 500 MHz, 300 K, in CDCl_3 with sample concentrations ranging from 2–10 mM.

Compound	$\Delta\delta$ [ppm]							
	H_{meso}	$\text{H}_{\beta 1}$	$\text{H}_{\beta 2}$	H_o	H_m	$\text{H}_{\text{N}\alpha}$	H_{Tz}	$\text{H}_{\text{C}\alpha}$
(TA) ₄ -Zn	–	–	–0.14	–0.08	–0.27	–0.35	–0.39	–0.83
(PS ₂₀) ₄ -Zn	–	–	–0.03	–0.03	–0.17 ^[a]	–0.23	–0.31 ^[a]	–0.56
(PS ₃₀) ₄ -Zn	–	–	–0.04	–0.05	–0.20 ^[a]	–0.26	–0.36 ^[a]	–0.58
(PS ₄₀) ₄ -Zn	–	–	–0.04	–0.05	–0.19 ^[a]	–0.26	–0.22 ^[a]	–0.64
(PBA ₁₅) ₄ -Zn	–	–	+0.01	0.00	–0.16	–0.22	–0.23	–0.60
(PrBA ₁₉) ₄ -Zn	–	–	+0.02	0.00	–0.12	–0.16	–0.16	–0.54
(PS ₂₀) ₂ -Zn	+0.10	–0.02	–0.09	–0.15	–0.31 ^[a]	–0.79	–0.41 ^[a]	–1.80
(PS ₃₀) ₂ -Zn	+0.11	0.04	–0.05	–0.12	–0.36 ^[a]	–0.51	–0.37 ^[a]	–1.26
(PS ₄₀) ₂ -Zn	+0.12	0.06	–0.02	–0.07	–0.30 ^[a]	–0.42	–0.41 ^[a]	–1.05

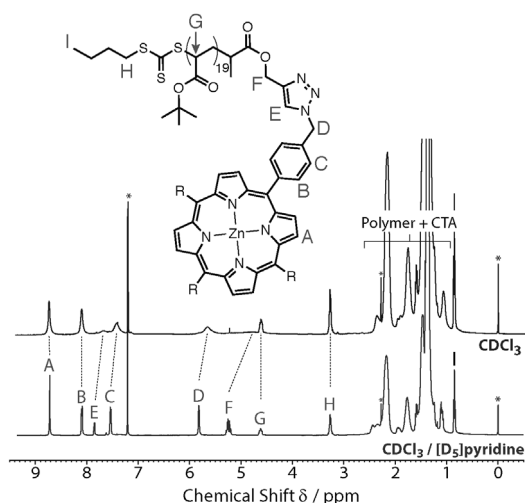


Figure 3. ^1H NMR spectra (500 MHz) of (PrBA₁₉)₄-Zn in CDCl_3 with and without $[\text{D}_5]$ pyridine (2% v/v). Assembly-induced shifting of signals C–F agree closely with the shifts observed for (TA)₄-Zn. Complex splitting of F is most likely due to diastereotopic induction by the nearby chiral center (see Supporting Information, Section S5.2). Assignments: A = $\text{H}_{\beta 1}$, B = H_o , C = H_m , D = $\text{H}_{\text{N}\alpha}$, E = H_{Tz} , F = $\text{H}_{\text{C}\alpha}$. Asterisks indicate residual solvent peaks.

samples (freeze-pump-thaw) did not improve the quality of the spectrum, while increasing the mixing time above 500 ms introduced spin-diffusion artifacts (Supporting Information, Figure S22), which are typical of high molecular weight compounds.^[34] We were unable to identify a set of NOESY parameters that provided readable intensity for the peaks undergoing chemical exchange ($\text{H}_{\text{C}\alpha}$ and $\text{H}_{\text{N}\alpha}$) while also preventing macromolecular spin-diffusion. Despite the limitations of the NOESY experiment, good agreement between the one-dimensional ^1H NMR spectra of the PPCs supports self-assembly via porphyrinatozinc–triazole coordination in each instance.

The Soret and *Q*-bands in the UV/Vis spectra of the PPCs were split into two populations when recorded in chloroform. The absorption spectrum of (PS₂₀)₄-Zn in chloroform is shown as an example (Figure 5). The dominant contributions to the broadened Soret band and *Q*-bands are typical of a zinc porphyrin without an axial substituent,^[35,36] whereas the red-shifted shoulder features are attributed to the porphyrinatozinc–triazole complex. As the

total concentration of the PPC was varied, the relative proportions of these two populations changed (Figure 6), indicating an equilibrium between unimers and self-assembled oligomers in solution.

To demonstrate that the red-shifted shoulder bands were indeed due to axial coordination of a basic ligand to the zinc porphyrin, the UV/Vis spectrum of (PS₂₀)₄-Zn was re-recorded in chloroform with 5 equiv of pyridine (Figure 5). A complete shift of the original Soret band from 421 to 430 nm indicates quantitative formation of the porphyrinatozinc–pyridine complex. Both the Soret and *Q*-bands shifted by approximately 500 cm^{-1} without any associated spectral broadening. Good agreement between the position of the shoulder feature and the peak wavelength of the porphyrinatozinc–pyridine complex suggests that the shoulder band in Figure 5 is due to self-association of the PPCs via porphyrinatozinc–triazole coordination.

Measurement of PPC association constant: Since the PPCs are multitopic subcomponents, self-assembly can yield step-growth supramolecular oligomers of the type shown in Scheme 2. We have modeled the self-assembly behaviour as an isodesmic oligomerisation process, whereby short linear structures are formed. The system illustrated in Scheme 1 is described by the addition of a single unimer unit to a supramolecular chain of length n , extending it to length $n + 1$:



which has the following equilibrium constant expression:

$$K = \frac{[\text{P}_{n+1}]}{[\text{P}_1][\text{P}_n]} \quad (3)$$

We do not expect any desolvation or pre-organisational effects to drive self-assembly in this system. The association constant is therefore assumed to be the same for the addition of each subunit. This “Equal-*K*” or *isodesmic* self-assembly behaviour is in direct contrast to *cooperative* self-assembly, which involves the initial unfavourable association of monomer units (nucleation) followed by favourable elongation to form large assemblies.^[37]

The concentration-dependent self-assembly of the PPCs was monitored by UV/Vis spectroscopy, observing character-

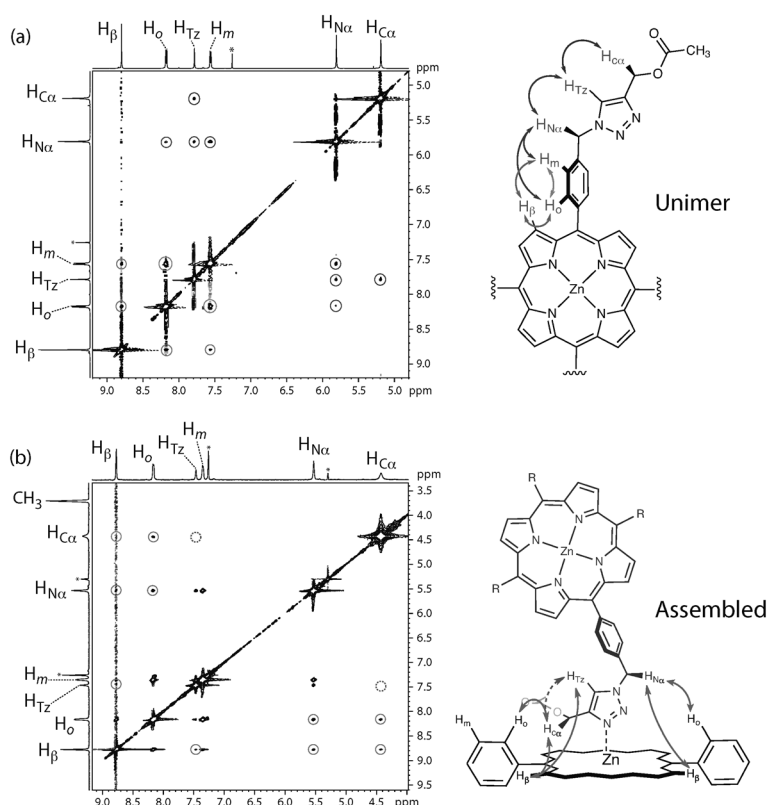


Figure 4. a) Partial NOESY spectrum of unimeric $(\text{TA})_4\text{-Zn}$ (10 mM in $\text{CDCl}_3/[\text{D}_2]$ pyridine, 98:2 v/v), 500 MHz, 500 ms mixing time). Key correlations along the porphyrin-phenylene-triazole arm are highlighted with arrows. Nearest-neighbour correlations, including an $\text{H}_\alpha\text{-H}_m$ COSY artifact, were observed. b) Partial NOESY spectrum of assembled $(\text{TA})_4\text{-Zn}$ (10 mM in CDCl_3 , 500 MHz, 500 ms mixing time). For clarity, only substituents involved in monotopic binding are shown. Key intermolecular NOE correlations (closed circles) support the proposed porphyrinatozinc-triazole complex. The $\text{H}_{\text{C}\alpha}\text{-H}_\beta$ correlation along the vertical axis was obscured by t_1 noise. The intramolecular $\text{H}_{\text{C}\alpha}\text{-H}_{\text{Tz}}$ correlation (dashed circle) was not observed.

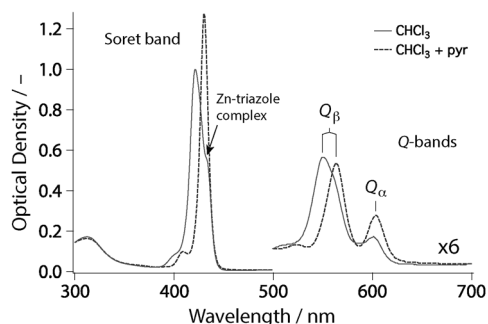


Figure 5. UV/Vis spectra of $(\text{PS}_{20})_4\text{-Zn}$ (ca. 5×10^{-5} M) in: CHCl_3 (solid line); and $\text{CHCl}_3 + 5$ equiv pyridine (dashed line). The spectrum in neat chloroform displays shoulder peaks at 420 and 560 nm, indicating partial self-assembly at this concentration.

istic changes in the lineshape of the Q_β absorption band due to zinc-triazole coordination. The UV/Vis spectra of $(\text{PS}_{20})_2\text{-Zn}$ in chloroform at different concentrations is shown as an example in Figure 6. The Q_β -band was analysed, rather than the Q_α or Soret bands, because the absorbance of the Soret band exceeded the saturation limit of the spectrophotometer at high concentrations, whereas the

absorbance of the Q_α -band was too weak at low concentrations.

Splitting of the Q_β -band results from a superposition of the spectra of porphyrinatozinc subunits with (“bound”) and without (“non-bound”) an axially-coordinated triazole unit. Bound porphyrins, indicated by unshaded porphyrin rings in Scheme 2, will invariably be constituents of the assembled structures; unbound porphyrins, shaded in grey in Scheme 2, can be either the chain-ends of the oligomers or free unimers. Since the UV/Vis spectra do not exhibit any excitonic coupling effects—evidenced by the narrow widths of the absorbance bands at the high and low concentration limits (Figure 6)—the observed spectrum is the sum of the component spectra.^[38] By applying a Gaussian multiple peak-fitting procedure to these spectra,^[39] the double-humped absorption feature was resolved into the Q_β -bands of the non-bound (high energy) and bound (low energy) zinc porphyrin chromophores (Supporting Information, Section S10). The peaks

and width of the fitted spectra were optimised to achieve a global fit at all concentrations.

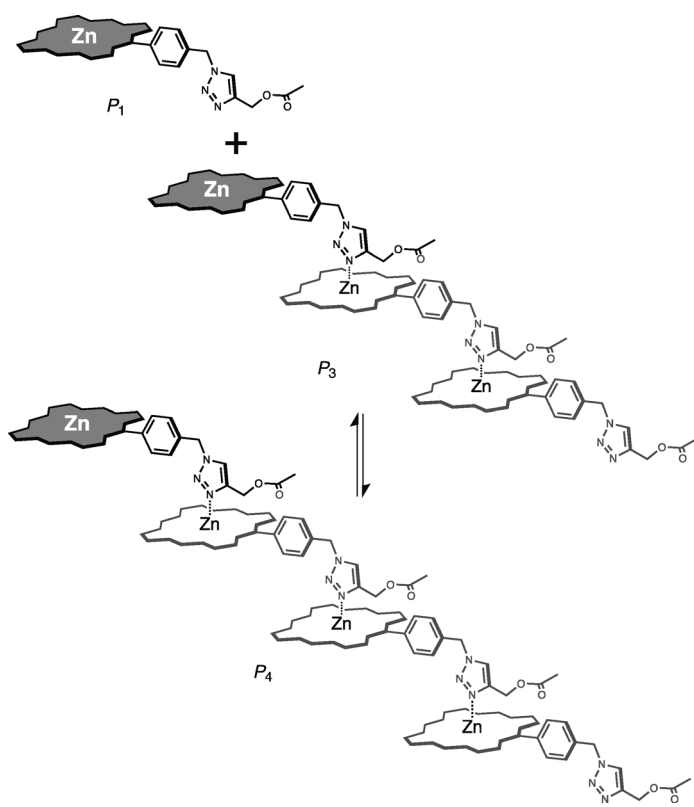
Association constants were calculated by fitting the isodesmic model described by Equation 4 to the concentration-dependent assembly data:

$$\theta_{\text{bound}} = \frac{(2C_T K + 1) - \sqrt{4C_T K + 1}}{2C_T K} \quad (4)$$

where θ_{bound} is the fraction of porphyrin moieties that have a bound triazole ligand, C_T is the total concentration of PPC (calculated using $M_{\text{n,theor}}$ from Table 1) and K is the association constant. The self-assembly model is derived in full in the Supporting Information (Section S11).^[40]

Influence of polymer chains on PPC association constant:

UV/Vis spectra of PPCs in chloroform at various concentrations were recorded and θ_{bound} was plotted as a function of total conjugate concentration (C_T) (Figure 7). Measured association constants are summarised in Table 3, with uncertainties estimated from non-linear regression analysis of the fitted model. Approximate degrees of supramolecular polymerisation (DP_N) were estimated from association constants



Scheme 2. Schematic representation of a linear supramolecular oligomerisation process via porphyrinatozinc–triazole coordination. Only the coordinating substituents are shown for clarity. Subunits are shaded according to the UV/Vis spectra that they will exhibit: grey subunits are the non-coordinated chromophores, and white (unshaded) subunits are those with an axially-coordinated triazole ligand.

using the method of Smulders et al.^[41] Supramolecular assemblies ranged in size from the dimer to the hexamer at the concentrations investigated in this study. Concentrations higher than 10 mM were not studied because the optical density of the porphyrin solutions exceeded the detection limit of the spectrophotometer. Fortunately, we were able to obtain assembly data over a sufficiently wide concentration range to measure the association constants.

Figure 7a shows the concentration-dependent assembly behaviour of $(\mathbf{TA})_4\text{-Zn}$ and the set of two-arm polystyrene conjugates with different arm lengths. $(\mathbf{TA})_4\text{-Zn}$ represents a PPC with a chain length of zero. While $(\mathbf{TA})_2\text{-Zn}$ would have provided an ideal comparison to the two-arm conjugates, its concentration-dependent behaviour could not be analysed due to its very low solubility in chloroform. Excellent agreement between the experimental data and the model described by Equation (4) supports an isodesmic self-assembly mechanism. The association constant of $(\mathbf{TA})_4\text{-Zn}$ ($K = 3.4 \pm 0.3 \times 10^4 \text{ M}^{-1}$) is of the same order of magnitude as other non-stabilised supramolecular porphyrin complexes based on zinc–triazole and zinc–pyridine coordination.^[32,42,43] The association constant decreased by 87% upon attachment of two PS_{20} chains ($K = 4.5 \pm 0.6 \times 10^3 \text{ M}^{-1}$), and continued to decrease by a further 82 and 59% as the chain length

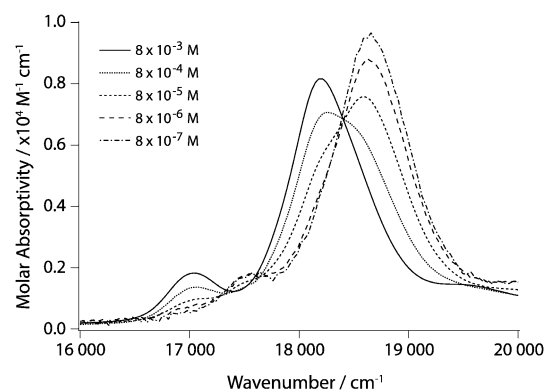


Figure 6. Q-band region of the $(\text{PS}_{20})_2\text{-Zn}$ UV/Vis spectra in CHCl_3 at various concentrations. Absorption data was converted to molar absorptivity [$\text{M}^{-1} \text{cm}^{-1}$] in order to negate the effect of using cuvettes with different path lengths.

Table 3. Association constants (K) of PPCs, and indicative values of the degree of supramolecular polymerisation (DP_N) at the maximum concentrations studied by UV/Vis.

Conjugate	K [M^{-1}]	C_T [mM]	DP_N
$(\mathbf{TA})_4\text{-Zn}$	$3.4 \pm 0.3 \times 10^4$	0.3	3.7
$(\text{PS}_{20})_2\text{-Zn}$	$4.5 \pm 0.6 \times 10^3$	7.5	6.3
$(\text{PS}_{30})_2\text{-Zn}$	$8.2 \pm 0.3 \times 10^2$	10	3.4
$(\text{PS}_{40})_2\text{-Zn}$	$3.5 \pm 0.1 \times 10^2$	6.8	2.1
$(\text{PS}_{20})_4\text{-Zn}$	$1.1 \pm 0.1 \times 10^3$	4.0	2.6
$(\text{PBA}_{15})_4\text{-Zn}$	$6.3 \pm 0.9 \times 10^2$	3.2	2.0
$(\text{PBA}_{19})_4\text{-Zn}$	$9.7 \pm 1.9 \times 10^2$	3.2	2.3

was increased to PS_{30} ($K = 8.2 \pm 0.3 \times 10^2 \text{ M}^{-1}$) and PS_{40} ($K = 3.5 \pm 0.1 \times 10^2 \text{ M}^{-1}$), respectively. The effect of increasing chain length exhibited a diminishing influence on the association constant as the polymer length was increased, suggesting that the polymer repeating units nearest to the porphyrin core have the greatest influence on steric shielding. Similar core shielding effects have been observed with porphyrin-cored star polymers.^[21,44]

The effect of changing grafting density (i.e., two or four grafted polymer arms) showed a similar trend to the arm length series, with the association constant decreasing as the degree of steric crowding around the porphyrin core increased (Figure 7b). Increasing the grafting density involves two competing factors: greater steric crowding around the porphyrin core, but also a larger number of triazole ligands within the PPC framework. The observed decrease in association constant with increasing grafting density implies that steric hindrance around the porphyrin core is the dominant factor. In similar work on steric protection of porphyrin-cored star polymers, Hecht et al. concluded that the number of arms grafted to the porphyrin core has little influence on the degree of steric shielding.^[44] In this instance, the authors were investigating porphyrin-cored stars with eight and sixteen grafted polymer arms, as opposed to the two- and four-arm conjugates presented herein. Since we observe a difference in association constant for grafting densities of two and four, the optimal grafting density for shielding the porphyrin

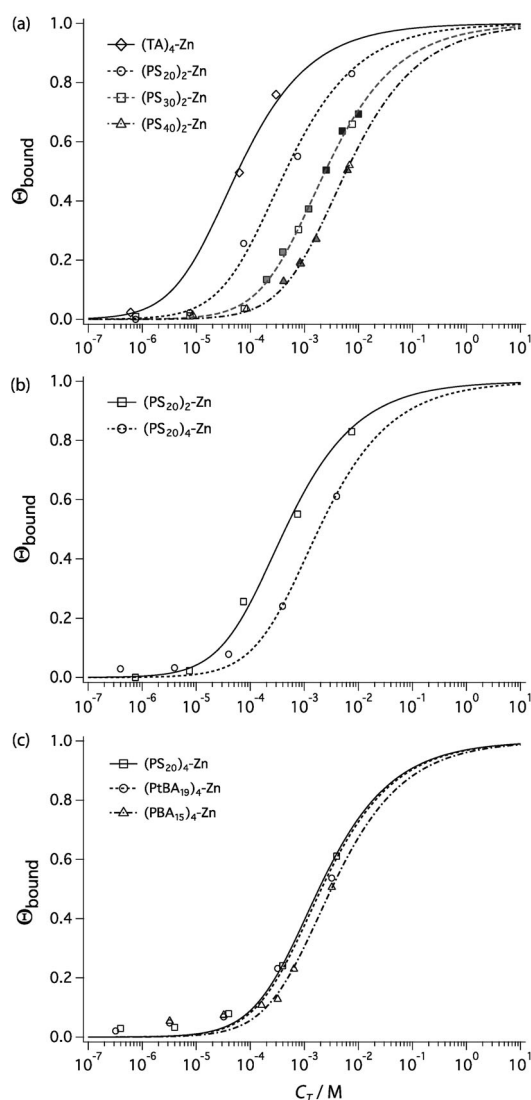


Figure 7. Concentration-dependent assembly curves of the PPCs. The fraction of bound chromophores (Θ_{bound}) is plotted against the total conjugate concentration (C_T). Experimental data are fitted to Equation (4). a) Arm length dependence. $(\text{TA})_4\text{-Zn}$ represents an effective chain length of zero. Shaded markers represent repetitions within a dataset. b) Grafting density dependence. c) Polymer repeating unit dependence.

core most probably lies between four and eight polymer arms. This is an important consideration when designing PPCs as supramolecular building blocks, as it is important to maintain steric access to the porphyrin core while also maximising the number of polymer chains that can be organised by a single supramolecular recognition motif. It is also useful to know the minimum number of polymer chains needed to sterically protect a porphyrin or other chromophore from excited-state quenching in solution.^[45]

We observed no significant difference between the association constants of PPCs with different polymer repeating units, suggesting that self-assembly is relatively insensitive to the steric bulk of the repeating unit (Figure 7c). Consequently, chemically-similar polymers with different bulk

properties—such as the polymers selected herein—are compatible with sterically-controlled self-assembly. It is important to note, also, that the isodesmic model fails to describe the assembly behaviour of the four-arm conjugates in Figure 7c at low concentrations ($C_T < 10^{-4}\text{M}$). The persistence of bound chromophores at low C_T suggests that there may be a barrier to disaggregation for the four-arm conjugates. The origin of this barrier is presently unknown, but could arise from steric shielding of the zinc–triazole interaction from solvent molecules in small (dimeric) PPC assemblies.

Effect of self-assembly on solid-state properties: The degree of supramolecular polymerisation is only appreciable at very high concentrations for an isodesmic assembly process.^[41] Since the highest concentration obtainable for a typical substance is that of the bulk material, we anticipated that self-assembly of the PPCs would manifest as a change in glass transition temperature (T_g) in the solid state.

Differential scanning calorimetry (DSC) was performed on $(\text{PS}_{20})_2\text{-Zn}$ and the freebase $(\text{PS}_{20})_2\text{-H}_2$ (Figure 8). The freebase conjugate was prepared directly from $(\text{PS}_{20})_2\text{-Zn}$ by acidic demetallation under mild conditions (Supporting Information, Section S6). Figure 8 shows that the T_g of the zinc conjugate was $\sim 6\text{K}$ higher than the freebase. We attribute the increase in T_g to self-assembly via the zinc–triazole assembly mode, which most likely cross-links the material in the bulk state

Conclusion

The marriage of molecular self-assembly and polymer chemistry offers numerous routes for building nanostructured soft materials with interesting dynamic behaviour. We have presented a modular strategy for synthesising triazole-linked porphyrin–polymer conjugates, which assemble into supramolecular assemblies via porphyrinatozinc–triazole coordination. By altering the polymer microenvironment around the porphyrin core we are able to systematically tune the as-

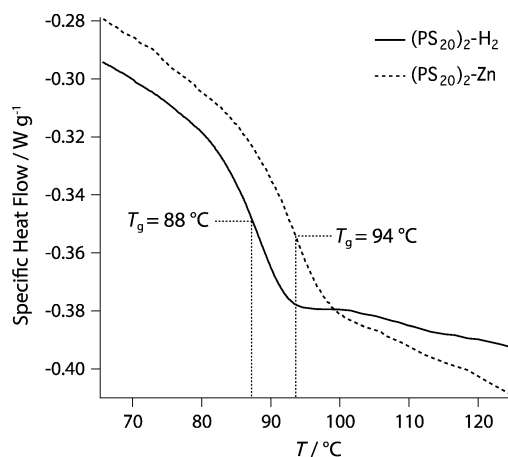


Figure 8. DSC traces of $(\text{PS}_{20})_2\text{-Zn}$ and $(\text{PS}_{20})_2\text{-H}_2$, with T_g values of 88 and 94 °C, respectively.

sociation constant of the porphyrinatozinc–triazole coordination complex, or switch it completely to the disassembled state by introducing a competitive ligand. Porphyrinatozinc–triazole coordination was shown to alter the properties of the bulk material, manifesting in a 6 K increase in the glass transition temperature of $(\text{PS}_{20})_2\text{-Zn}$. We envisage that the multitopic design of the PPCs may stabilise the tertiary structure of larger supramolecular assemblies due to potential preorganisational effects. Furthermore, the inter-chromophore distances between the porphyrin subunits may be sufficiently small to enable light-mediated energy-transfer processes along the porphyrinatozinc–triazole backbone. Consequently, PPCs containing ruthenium and cobalt metalloporphyrin cores are currently being investigated for constructing larger, more stable PPC arrays with potentially interesting photophysical properties.

Experimental Section

Additional experimental information, characterisation data, assignment of ^1H , ^{13}C , HSQC, HMBC and NOESY NMR spectra, analytical GPC traces, UV/Vis spectra, model derivation and self-assembly analysis are included in the Supporting Information.

Materials: Commercial solvents and reagents were used without further purification unless specified otherwise. 2-(Butylthiocarbonothioylthio)propanoic acid (PABTC) and 2,2'-azobisisobutyronitrile were received from DuluxGroup Australia. (Prop-2-ynyl propanoate)yl butyl trithiocarbonate (PYPBTC) RAFT agent was synthesised by Dr. Raphael Barbey (KCPC, The University of Sydney, Australia) using a procedure based on that of Konkolewicz et al.^[18] Tetrahydrofuran (THF) was distilled from the sodium/benzophenone ketyl under N_2 to remove water and the inhibitor (4-hydroxy-3,5-di-*tert*-butyltoluene). Liquid styrene was passed over basic alumina prior to polymerisation to remove the inhibitor. 2,3-Dichloro-5,6-dicyano-1,4-benzoquinone (DDQ) was recrystallised from CHCl_3 and dried under vacuum prior to use.^[46] Pyrrole was distilled from calcium hydride under reduced pressure and stored under nitrogen; distilled pyrrole was passed through alumina immediately prior to use. Chlorobenzene was distilled from CaCl_2 under reduced pressure and canulated directly into the reaction vessel under N_2 .

Methods: Microwave syntheses were performed on an A.I. Scientific CEM Discover S-Class synthesis microwave using 5 mL borosilicate sealable microwave tubes. Preparative size-exclusion chromatography (SEC) was conducted using a gravity fed column (3 cm internal diameter \times 40 cm) containing Bio-Rad Biobeads S-X1 cross-linked polystyrene size-exclusion matrix using toluene as the eluent (flow rate 0.5 mL min⁻¹). Optical absorption spectroscopy was performed at 295 K on a Varian Cary 4000 UV-visible spectrophotometer operating in double beam mode with air in the reference path. Temperature of the samples was controlled using an Agilent Technologies Cary Peltier-type temperature controller. Samples were analysed using quartz cuvettes with optical path lengths of 1 cm, 2 mm, 1 mm or 0.1 mm (demountable), depending on the concentration of the porphyrin solution. Electrospray ionisation (ESI) mass spectra were recorded on a ThermoQuest Finnigan LCQ ion trap mass spectrometer. High resolution ESI and matrix-assisted laser desorption/ionisation Fourier transform ion cyclotron resonance (MALDI-FTICR) mass spectra were recorded on a Bruker Daltonics 7T FTICR Mass Spectrometer. No additional matrix was required for porphyrin-containing samples. Attenuated Total Reflection (ATR) infrared spectra were recorded on a Bruker Alpha-E ATR spectrometer fitted with a zinc–selenide crystal. Diffuse Reflectance Infrared Fourier Transform Spectroscopy (DRIFTS) was performed on a Varian 800 Scimitar Series FT-IR spectrometer. Spectra were recorded with a resolution of 4 cm⁻¹ for 16 repetitions. Molecular weight distributions of polymers were measured by ana-

lytical gel permeation chromatography (GPC) on a Shimadzu LC-10AT liquid chromatography system fitted with a PLgel 5 μm MiniMIX-C (50 \times 4.6 mm) guard column and two PLgel 5 μm MIXED-C (300 \times 7.5 mm) columns. The system was equipped with a Shimadzu RID-10A differential refractive index detector and a Shimadzu SPD-10 A UV-visible absorption detector. THF containing 1,4-hydroquinone (0.04 g L⁻¹) was used as the mobile phase, eluting at 1.0 mL min⁻¹ at 40 °C. Analyte samples were dissolved in THF spiked with 0.5 vol% toluene as the flow rate marker and filtered through a polytetrafluoroethylene filter (0.45 μm pore size) prior to injection (100 μL loop volume). Chromatograms were calibrated using linear polystyrene standards. Experimental molecular weight (M_n) and dispersity (D) values of the synthesised polymers were determined by conventional calibration using Cirrus software. 1D ^1H NMR spectra were recorded at 300 K on a Bruker Avance DPX 200 (200 MHz), DPX 300 (300 MHz) or DPX 500 MHz NMR spectrometer using tetramethylsilane (TMS) as the internal reference. Signals are recorded in terms of chemical shift (in ppm), relative integral, multiplicity, coupling constants (in Hz) and assignment, in that order. The following abbreviations for multiplicity are used: s, singlet; d, doublet; t, triplet; m, multiplet; br, broad. Deuterated solvents were purchased from Cambridge Isotope Laboratories, Inc., and stored away from light at room temperature. Deuterated chloroform was de-acidified by passage through basic alumina (Brockmann Grade I) immediately prior to use. Samples were filtered through a plug of dry cotton wool directly into NMR tubes prior to analysis to remove any suspended solids. Two-dimensional ^1H NMR spectra were recorded at 300 K on a Bruker Avance DPX 500 MHz NMR spectrometer, using a BBO two-channel probe that was automatically tuned and matched to the correct operating frequencies (^1H and ^{13}C). Pulse calibration (90°) was routinely performed for ^1H experiments (typically $\sim 12.3 \mu\text{s}$ at 15.488 W), and T_1 values were estimated by the inversion-recovery method using the standard Bruker pulse program *t1r1d*. Spectra were processed using Varian Topspin 3 and MestreNova Lite software. Two-dimensional NOESY spectra were recorded on a Bruker Avance DPX 500 MHz spectrometer using the standard Bruker program *noesygptp*. At least three different mixing times ranging from 100 to 500 ms were tested to ensure optimal discrimination between direct cross-relaxation and spin-diffusion and to estimate the mixing time range where the initial rate approximation holds. Spectra were acquired at 300 K with 2048 data points in f_2 . Typically 8 scans were accumulated for 512 increments in f_1 . Phase and baseline corrections were applied along both axes, and excessive t_1 noise was removed by subtracting 1D projections of the random noise from a correlation-free region of the 2D spectra. All data processing was performed using Bruker Topspin 3.0 software. Differential scanning calorimetry (DSC) was performed using a TA Instruments DSC 2920 modulated calorimeter, calibrated using an indium metal standard. Samples (5–10 mg) were heated in a tared aluminium pan from 25 to 300 °C under a nitrogen atmosphere (60 cm³ min⁻¹). Samples were then cooled to 0 °C before being heated to 300 °C at a rate of 10 °C min⁻¹. This cycle of cooling and reheating was performed 3 times. An empty aluminium pan was used as a reference. The glass transition temperature (T_g) was determined at the stationary point on the first derivative curve of the heating cycle data.

Zinc(II) tetra(triazolyl acetate)porphyrin, (TA)₄-Zn: A 5 mL microwave tube was charged with $\text{TN}_3\text{PP-Zn}$ (10 mg, 11 μmol), sodium ascorbate (4.4 mg, 22 μmol), propargyl acetate (1.48 mL, 60 mm solution in THF), copper(II) sulfate (1.1 mg, 4.5 μmol), and DMF (2 mL). The contents of the tube were sonicated briefly to obtain a homogeneous purple solution, then a magnetic stirrer bar was added and the tube sealed. The reaction was heated under microwave irradiation (100 W, 100 °C) for 25 min, then allowed to cool to room temperature. The solvent was removed by rotary evaporation and the purple residue was redissolved in a minimal amount of CH_2Cl_2 with 5% *v/v* pyridine and passed through a short alumina column to remove any remaining copper salts. After removal of the solvents, the product was obtained as shiny purple microcrystals (14.1 mg, 98%). M.p. > 300 °C; ^1H NMR (500 MHz, $\text{CDCl}_3/\text{TMS} + 2\% \text{ v/v } [\text{D}_3]\text{pyridine}$): $\delta = 8.84$ (s, 8H, β -pyrrolic H), 8.18 (d, $J = 8.0$ Hz, 8H, phenyl H_a), 7.85 (s, 4H, triazole H), 7.60 (d, $J = 8.0$ Hz, 8H, phenyl H_b), 5.86 (s, 8H, N_α -triazole CH_2), 5.31 (s, 8H, C_α -triazole CH_2), 2.12 ppm (s, 12H, acetate CH_3); ^{13}C NMR (125 MHz, $\text{CDCl}_3/\text{TMS} + 2\% \text{ v/v}$

[D₅]pyridine): δ = 171.1 (acetate C=O), 150.0 (α -pyrrole), 144.1 (phenyl C_{ipso}), 143.6 (triazole C₄), 135.3 (phenyl C_{ortho}), 133.6 (phenyl C_{para}), 131.8 (β -pyrrole), 126.1 (phenyl C_{meta}), 124.1 (triazole C₅), 119.8 (porphyrin C_{meso}), 57.8 (triazole-H_{Ca}), 54.3 (triazole-H_{Na}), 21.0 ppm (acetate CH₃); IR (ATR, solid film): ν_{\max} = 2923, 2852, 2246, 1736, 1223, 993, 906, 796, 782, 720, 646 cm⁻¹; UV/Vis (0.124 M pyridine in CHCl₃): λ_{\max} (log₁₀(ϵ)) = 409 (4.64), 430 (5.71), 563 (4.29), 603 nm (4.02); UV/Vis (CHCl₃): λ_{\max} (log₁₀(ϵ)) = 400 (4.57), 420 (5.66), 548 (4.30), 586 nm (3.68); HRMS (MALDI-FTICR): m/z : calcd for: 1311.36507; found: 1311.36537 [M+Na]⁺; MS (MALDI-FTICR): m/z (%): 1311.37 [M+Na]⁺ (20), 1249.45 [M+H-C₂H₅O]⁺ (100), 1227.47 [M-Zn]⁺ (40).

Zinc(II) di(triazolyl acetate)porphyrin, (TA)₂-Zn: A 5 mL microwave tube was charged with **DN₃PP-Zn** (10.0 mg, 15.7 μ mol), sodium ascorbate (5.5 mg, 28 μ mol), propargyl acetate (0.37 mL, 95 mM solution in THF), copper(II) sulfate (1.2 mg, 4.7 μ mol), and DMF (2 mL). The content of the tube was sonicated briefly to obtain a homogeneous purple solution, then a magnetic stirrer bar was added and the tube sealed. The reaction was heated under microwave irradiation (100 W, 100 °C) for 25 min, then allowed to cool to room temperature. Work-up was performed as for **(TA)₄-Zn** to yield the product as a dark purple solid residue (12.5 mg, 97%). M.p. >300 °C; ¹H NMR (500 MHz, CDCl₃/TMS + 15% v/v [D₅]pyridine): δ = 10.23 (s, 2H, meso-H), 9.38 (d, J = 4.5 Hz, 4H, β -pyrrolic H), meso-H), 9.03 (d, J = 4.5 Hz, 4H, β -pyrrolic H), 8.24 (d, J = 8.0 Hz, 4H, phenyl H_o), 7.93 (s, 2H, triazole H), 7.65 (d, J = 8.0 Hz, 4H, phenyl H_m), 5.88 (s, 4H, N_a-triazole CH₂), 5.35 (s, 4H, C_a-triazole CH₂), 2.13 ppm (s, 6H, acetate CH₃); ¹³C NMR (125 MHz, CDCl₃/TMS + 15% v/v [D₅]pyridine): δ = 170.9 (acetate C=O), 149.7 (pyrrole), 149.5 (pyrrole), 144.0 (phenyl C_{ipso}), 143.5 (triazole C₄), 133.5 (phenyl C_{ortho}), 132.0 (phenyl C_{para}), 131.8 (pyrrole), 126.1 (phenyl C_{meta}), 124.0 (triazole C₅), 118.4 (porphyrin C_{meso}), 106.0 (pyrrole), 57.8 (triazole-H_{Ca}), 54.3 (triazole-H_{Na}), 20.9 ppm (acetate CH₃); IR (DRIFTS, KBr matrix): ν_{\max} = 2923, 2852, 1739, 1518, 1439, 1394, 1366, 1236, 1146, 1119, 1058, 996, 850, 823, 781, 729, 702 cm⁻¹; UV/Vis (THF): λ_{\max} (log₁₀(ϵ)) = 313 (4.25), 353 (4.05), 393, (4.63), 413 (5.72), 451 (3.19), 504 (3.45), 543 (4.31), 581 nm (3.54); HRMS (MALDI-FTICR): m/z : calcd for: 831.21287; found: 831.21236 [M+H]⁺; MS (MALDI-FTICR): m/z (%): 831.21 [M+H]⁺ (10), 747.53 [M+H-2xCOCH₃]⁺ (100).

General Procedure for PPC synthesis: Synthesis of **(PS₃₀)₄-Zn** is described. Azidoporphyrin **TN₃PP-Zn** (10 mg, 11 μ mol), alkyne-functionalised RAFT polystyrene (DP = 30, 147 mg, 49.0 μ mol), copper(II) sulfate pentahydrate (1.7 mg, 6.7 μ mol) and sodium ascorbate (7.7 mg, 39 μ mol) were weighed into a 5 mL sealable microwave tube. DMF (3 mL) and a magnetic stirrer bar was added and the vessel sealed. The reaction mixture was sonicated briefly, then heated under microwave irradiation (100 W, 100 °C) for 25 min then allowed to cool. Work-up procedure consisted of passing the crude reaction mixture directly through a short alumina column (Brockmann grade I), then diluting with ethyl acetate (ca. 20 mL) and washing the organic phase with deionised water (5 x 50 mL) to remove the DMF. The organic layer was dried over Na₂SO₄, filtered and the solvents removed on a rotary evaporator. The resulting amorphous purple solid was dissolved in minimal CH₂Cl₂ and precipitated by dropwise addition into methanol at -78 °C to afford the purified polymer as a pale purple powder. For two-arm conjugates, the amount of polymer, catalyst and reducing agent was halved, but reaction volume remained constant.

(PS₃₀)₄-Zn: $M_{n,GPC}$ (THF) = 9400 g mol⁻¹; D = 1.30; ¹H NMR (500 MHz, CDCl₃/TMS + 2% v/v [D₅]pyridine): δ = 8.77 (brs, 8H, β -pyrrolic H), 8.14 (d, J = 7.5 Hz, 8H, phenyl H_o), 7.67 (brm, 4H, triazole Ar-H), 7.53 (d, J = 7.5 Hz, phenyl 8H, H_m), 7.25–6.25 (brm, 400H, polystyrene Ar-H), 5.78 (brm, 8H, triazole-H_{Na}), 5.12 (brm, 8H, triazole-H_{Ca}), 4.90–4.71 (brm, 4H, -CH-SCS₂-), 3.25 (brs, 8H, -SCH₂CH₂-), 1.86–1.08 (brm, 238H, backbone -CH₂CH- and -S-CH₂[CH₂]CH₃), 0.90 ppm (brm, 24H, -S(CH₂)₃-CH₃ and -O(C=O)CHCH₃); IR (DRIFTS, KBr matrix): ν_{\max} = 3079, 3061, 3025, 2924, 2852, 1944, 1873, 1804, 1734, 1601, 1493, 1450, 1157, 1028, 906, 756, 698, 540 cm⁻¹; UV/Vis (THF): λ_{\max} (log₁₀(ϵ)) = 311 (4.76), 404 (4.57), 425 (5.66), 486 (3.26), 517 (3.50), 557 (4.25), 595 (3.82), 643 nm (2.6).

(PS₃₀)₄-Zn: $M_{n,GPC}$ (THF) = 10790 g mol⁻¹; D = 1.26; ¹H NMR (500 MHz, CDCl₃/TMS + 2% v/v [D₅]pyridine): δ = 8.78 (brs, 8H, β -pyrrolic H), 8.16 (d, J = 6.8 Hz, 8H, phenyl H_o), 7.69 (brm, 4H, triazole Ar-H), 7.54 (d, J = 6.7 Hz, 8H, phenyl H_m), 7.32–6.27 (brm, 600H, polystyrene Ar-H), 5.79 (brm, 8H, triazole-H_{Na}), 5.12 (brm, 8H, triazole-H_{Ca}), 5.01–4.70 (brm, 4H, -CH-SCS₂-), 3.26 (brs, 8H, -SCH₂CH₂-), 2.53–1.20 (brm, 358H, backbone -CH₂CH- and -S-CH₂[CH₂]CH₃), 0.92 ppm (brm, 24H, -S(CH₂)₃-CH₃ and -O(C=O)CHCH₃); IR (DRIFTS, KBr matrix): ν_{\max} = 3077, 3060, 3025, 2924, 2852, 1944, 1874, 1804, 1734, 1601, 1493, 1452, 1157, 1028, 908, 756, 698 cm⁻¹; UV/Vis (THF): λ_{\max} (log₁₀(ϵ)) = 312 (4.75), 404 (4.56), 425 (5.67), 484 (3.26), 518 (3.47), 557 (4.24), 596 nm (3.81).

(PS₃₀)₄-Zn: $M_{n,GPC}$ (THF) = 15250 g mol⁻¹; D = 1.25; ¹H NMR (300 MHz, CDCl₃/TMS + 2% v/v [D₅]pyridine): δ = 8.77 (brs, 8H, β -pyrrolic H), 8.13 (brs, 8H, phenyl H_o), 7.67 (brm, 4H, triazole Ar-H), 7.51 (brs, 8H, phenyl H_m), 7.25–6.25 (brm, 800H, polystyrene Ar-H), 5.76 (brm, 8H, triazole-H_{Na}), 5.11–5.00 (brm, 8H, triazole-H_{Ca}), 4.87–4.73 (brm, 4H, -CH-SCS₂-), 3.24 (brs, 8H, -SCH₂CH₂-), 1.86–1.08 (brm, 478H, backbone -CH₂CH- and -S-CH₂[CH₂]CH₃), 0.90 ppm (brm, 24H, -S(CH₂)₃-CH₃ and -O(C=O)CHCH₃); IR (DRIFTS, KBr matrix): ν_{\max} = 3077, 3060, 3025, 2924, 2852, 1944, 1874, 1805, 1734, 1601, 1493, 1452, 1157, 1028, 756, 698 cm⁻¹; UV/Vis (THF): λ_{\max} (log₁₀(ϵ)) = 312 (4.74), 404 (4.56), 425 (5.67), 485 (3.27), 517 (3.48), 557 (4.24), 596 (3.81), 642 nm (2.48).

(PS₂₀)₂-Zn: $M_{n,GPC}$ (THF) = 5170 g mol⁻¹; D = 1.18; ¹H NMR (500 MHz, CDCl₃/TMS + 2% v/v [D₅]pyridine): δ = 10.23 (s, 2H, porphyrin meso-H), 9.37 (brs, 4H, β -pyrrolic H), 9.01 (brm, 4H, β -pyrrolic H), 8.24 (brm, 4H, phenyl H_o), 7.71 (brm, 2H, triazole Ar-H), 7.61 (brs, 4H, phenyl H_m), 7.45–6.30 (brm, 200H, polystyrene Ar-H), 5.84 (brm, 4H, triazole-H_{Na}), 5.18 (brm, 4H, triazole-H_{Ca}), 4.97–4.72 (brm, 2H, -CH-SCS₂-), 3.27 (brs, 4H, -SCH₂CH₂-), 2.58–1.16 (brm, 124H, backbone -CH₂CH- and -S-CH₂[CH₂]CH₃), 0.92 ppm (brm, 12H, -S(CH₂)₃-CH₃ and -O(C=O)CHCH₃); IR (DRIFTS, KBr matrix): ν_{\max} = 3080, 3061, 3025, 2926, 1944, 1870, 1804, 1735, 1600, 1493, 1453, 1370, 1157, 1066, 1027, 999, 907, 757, 699 cm⁻¹; UV/Vis (THF): λ_{\max} (log₁₀(ϵ)) = 312 (4.37), 392 (4.42), 413 (5.47), 451 (3.57), 505 (3.40), 543 (4.12), 580 (3.40), 633 nm (2.73).

(PS₃₀)₂-Zn: $M_{n,GPC}$ (THF) = 7150 g mol⁻¹; D = 1.19; ¹H NMR (500 MHz, CDCl₃/TMS + 2% v/v [D₅]pyridine): δ = 10.13 (s, 2H, porphyrin meso-H), 9.27 (brs, 4H, β -pyrrolic H), 8.91 (brm, 4H, β -pyrrolic H), 8.15 (brm, 4H, phenyl H_o), 7.63 (brm, 2H, triazole Ar-H), 7.52 (brs, 4H, phenyl H_m), 7.17–6.30 (brm, 300H, polystyrene Ar-H), 5.75 (brm, 4H, triazole-H_{Na}), 5.07 (brm, 4H, triazole-H_{Ca}), 4.97–4.72 (brm, 2H, -CH-SCS₂-), 3.17 (brs, 4H, -SCH₂CH₂-), 2.58–1.16 (brm, 184H, backbone -CH₂CH- and -S-CH₂[CH₂]CH₃), 0.80 ppm (brm, 12H, -S(CH₂)₃-CH₃ and -O(C=O)CHCH₃); IR (DRIFTS, KBr matrix): ν_{\max} = 3080, 3061, 3025, 2926, 1944, 1870, 1804, 1735, 1600, 1493, 1453, 1370, 1157, 1066, 1027, 999, 907, 757, 699 cm⁻¹; UV/Vis (THF): λ_{\max} (log₁₀(ϵ)) = 312 (4.37), 393 (4.31), 413 (5.38), 451 (3.41), 505 (3.34), 543 (4.02), 580 (3.35), 634 nm (2.89).

(PS₄₀)₂-Zn: $M_{n,GPC}$ (THF) = 10200 g mol⁻¹; D = 1.25; ¹H NMR (500 MHz, CDCl₃/TMS + 2% v/v [D₅]pyridine): δ = 10.13 (s, 2H, porphyrin meso-H), 9.27 (brs, 4H, β -pyrrolic H), 8.91 (brm, 4H, β -pyrrolic H), 8.15 (brd, J = 6.7 Hz, 4H, phenyl H_o), 7.63 (brm, 2H, triazole Ar-H), 7.53 (brd, J = 7.0 Hz, 4H, phenyl H_m), 7.24–6.16 (brm, 400H, polystyrene Ar-H), 5.75 (brm, 4H, triazole-H_{Na}), 5.07 (brm, 4H, triazole-H_{Ca}), 4.97–4.72 (brm, 2H, -CH-SCS₂-), 3.17 (brs, 4H, -SCH₂CH₂-), 2.58–1.16 (brm, 184H, backbone -CH₂CH- and -S-CH₂[CH₂]CH₃), 0.80 ppm (brm, 12H, -S(CH₂)₃-CH₃ and -O(C=O)CHCH₃); IR (DRIFTS, KBr matrix): ν_{\max} = 3082, 3060, 3024, 2924, 1945, 1866, 1803, 1735, 1601, 1493, 1452, 1369, 1154, 1068, 1028, 998, 905, 758, 698 cm⁻¹; UV/Vis (THF): λ_{\max} (log₁₀(ϵ)) = 312 (4.36), 393 (4.30), 413 (5.37), 451 (3.40), 506 (3.34), 543 (4.02), 580 (3.34), 633 nm (2.89).

(PBA₁₅)₄-Zn: $M_{n,GPC}$ (THF) = 9190 g mol⁻¹; D = 1.24; ¹H NMR (500 MHz, CDCl₃/TMS + 2% v/v [D₅]pyridine): δ = 8.72 (s, 8H, β -pyrrolic H), 8.10 (d, J = 7.0 Hz, 8H, phenyl H_o), 7.84 (brm, 4H, triazole Ar-H), 7.54 (d, J = 7.4 Hz, 8H, phenyl H_m), 5.82 (d, J = 6.15 Hz, 8H, triazole-H_{Na}), 5.25 (brm, 8H, triazole-H_{Ca}), 4.75 (brm, 4H, -CH-SCS₂-), 3.97 (brs, 120H, butyl acrylate α -CH₂-), 3.27 (t, J = 7.5 Hz, 8H, -SCH₂CH₂-), 2.54–1.17 (brm, 436H, backbone -CH₂CH- and -S-CH₂[CH₂]CH₃ and

butyl acrylate β,γ -CH₂), 1.09 (t, $J=6.9$ Hz, 12H, -O(C=O)CHCH₃), 0.93 ppm (brs, 192H, -S(CH₂)₃-CH₃ and butyl acrylate -CH₃); IR (DRIFTS, KBr matrix): ν_{\max} = 2960, 2880, 1736, 1730, 1460, 1395, 1380, 1241, 1166, 1117, 1064, 943, 906, 837, 737 cm⁻¹; UV/Vis (THF): λ_{\max} (log₁₀(ϵ)) = 310 (4.75), 404 (4.59), 425 (5.66), 486 (3.48), 517 (3.56), 557 (4.26), 596 (3.86), 644 nm (2.98).

(**PtBA**)₄-**Zn**: $M_{n,GPC}$ (THF) = 11810 g mol⁻¹; $D=1.20$; ¹H NMR (500 MHz, CDCl₃/TMS + 2% v/v [D₃]pyridine): δ = 8.72 (s, 8H, β -pyrrolic H), 8.10 (d, $J=7.5$ Hz, 8H, phenyl H_o), 7.84 (brm, 4H, triazole Ar-H), 7.54 (d, $J=7.4$ Hz, 8H, phenyl H_m), 5.82 (brs, 8H, triazole-H_{Na}), 5.24 (m, 8H, triazole-H_{Ca}), 4.62 (m, 4H, -CH-SCS₂), 3.27 (m, 8H, -SCH₂CH₂-), 2.56–1.15 (buried, 16H, -S-CH₂[CH₂]CH₃), 2.17 (brs, 152H, backbone -CH₂-), 1.77 (brs, 76H, backbone -CH-), 1.37 (brs, 684H, *t*Bu-H), 1.09 (t, $J=7.4$ Hz, 12H, -O(C=O)CHCH₃), 0.85 ppm (t, $J=7.4$ Hz, 12H, -S(CH₂)₃-CH₃); IR (DRIFTS, KBr matrix): ν_{\max} = 2920, 2880, 1736, 1722, 1480, 1460, 1366, 1250, 1150, 906, 840 cm⁻¹; UV/Vis (THF): λ_{\max} (log₁₀(ϵ)) = 310 (4.73), 404 (4.58), 425 (5.66), 486 (3.48), 517 (3.55), 557 (4.26), 596 nm (3.86).

Acknowledgements

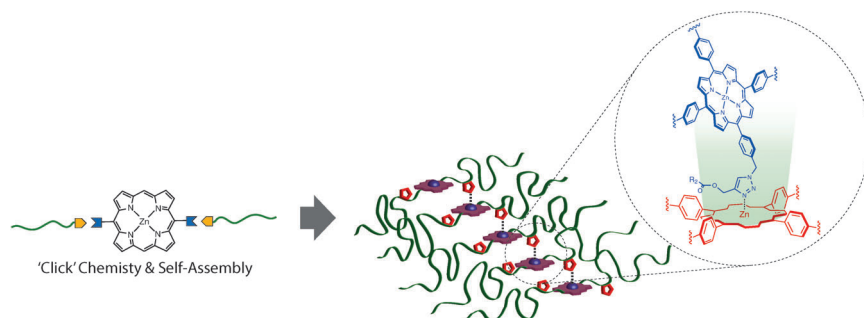
The authors acknowledge Dr. Algi Serelis of DuluxGroup for providing the RAFT agent, and Dr. Robert Chapman, Dr. Maarten Danial and Dr. Raphael Barbey for providing alkyne-functionalised polymers. D.A.R. acknowledges the Australian Government for an Australian Postgraduate Award and the University of Sydney for the Vice Chancellor's Research Scholarship. M.J.C. acknowledges the Australian Research Council Discovery Project grant DP1092560 for funding. S.P. acknowledges funding from the Australian Research Council Future Fellowship and Discovery programs.

- [1] a) J.-M. Lehn, *Angew. Chem.* **1990**, *102*, 1347–1362; *Angew. Chem. Int. Ed. Engl.* **1990**, *29*, 1304–1319; b) G. M. Whitesides, E. E. Simanek, J. P. Mathias, C. T. Seto, D. Chin, M. Mammen, D. M. Gordon, *Acc. Chem. Res.* **1995**, *28*, 37–44; c) G. R. Desiraju, *Nature* **2001**, *412*, 397–400; d) W. Lu, C. M. Lieber, *Nat. Mater.* **2007**, *6*, 841–850; e) K. R. Carter, *J. Mater. Chem.* **2011**, *21*, 14095–14096.
- [2] K. Matyjaszewski, in *Controlled Radical Polymerization*, American Chemical Society, **1998**, Vol. 685, pp. 2–30.
- [3] a) S.-L. Li, T. Xiao, C. Lin, L. Wang, *Chem. Soc. Rev.* **2012**, *41*, 5950–5968; b) N. Ayres, M. Weck, *Polym. Chem.* **2012**, *3*, 3031–3032; c) F. Huang, O. A. Scherman, *Chem. Soc. Rev.* **2012**, *41*, 5879–5880.
- [4] a) T. Terashima, T. Mes, T. F. A. De Greef, M. A. J. Gillissen, P. Besenius, A. R. A. Palmans, E. W. Meijer, *J. Am. Chem. Soc.* **2011**, *133*, 4742–4745; b) M. A. J. Gillissen, I. K. Voets, E. W. Meijer, A. R. A. Palmans, *Polym. Chem.* **2012**, *3*, 3166–3174; c) R. Chapman, M. L. Koh, G. G. Warr, K. A. Jolliffe, S. Perrier, *Chem. Sci.* **2013**, *4*, 2581–2589.
- [5] a) P. Cordier, F. Tournilhac, C. Soulie-Ziakovic, L. Leibler, *Nature* **2008**, *451*, 977–980; b) E. B. Berda, E. J. Foster, E. W. Meijer, *Macromolecules* **2010**, *43*, 1430–1437; c) P. Besenius, G. Portale, P. H. H. Bomans, H. M. Janssen, A. R. A. Palmans, E. W. Meijer, *Proc. Natl. Acad. Sci. USA* **2010**, *107*, 17888–17893; d) T. Mes, R. van der Weegen, A. R. A. Palmans, E. W. Meijer, *Angew. Chem.* **2011**, *123*, 5191–5195; *Angew. Chem. Int. Ed.* **2011**, *50*, 5085–5089; e) O. Altintas, U. Tunca, C. Barner-Kowollik, *Polym. Chem.* **2011**, *2*, 1146–1155; f) O. Altintas, E. Lejeune, P. Gerstel, C. Barner-Kowollik, *Polym. Chem.* **2012**, *3*, 640–651.
- [6] a) N. Nishiyama, M. Yokoyama, T. Aoyagi, T. Okano, Y. Sakurai, K. Kataoka, *Langmuir* **1998**, *14*, 377–383; b) S. N. Dublin, V. P. Conticello, *J. Am. Chem. Soc.* **2007**, *129*, 49–51; c) D. E. Przybyla, J. Chmielewski, *J. Am. Chem. Soc.* **2008**, *130*, 12610–12611; d) F. Grimm, N. Ulm, F. Gröhn, J. Düring, A. Hirsch, *Chem. Eur. J.* **2011**, *17*, 9478–9488.
- [7] a) S. Burattini, H. M. Colquhoun, J. D. Fox, D. Friedmann, B. W. Greenland, P. J. F. Harris, W. Hayes, M. E. Mackay, S. J. Rowan, *Chem. Commun.* **2009**, 6717–6719; b) S. Burattini, B. W. Greenland, D. H. Merino, W. Weng, J. Seppala, H. M. Colquhoun, W. Hayes, M. E. Mackay, I. W. Hamley, S. J. Rowan, *J. Am. Chem. Soc.* **2010**, *132*, 12051–12058; c) B. W. Greenland, M. B. Bird, S. Burattini, R. Cramer, R. K. O'Reilly, J. P. Patterson, W. Hayes, C. J. Cardin, H. M. Colquhoun, *Chem. Commun.* **2013**, *49*, 454–456.
- [8] a) J. Stadermann, H. Komber, M. Erber, F. Däbritz, H. Ritter, B. Voit, *Macromolecules* **2011**, *44*, 3250–3259; b) Q. Fu, J. M. Ren, G. G. Qiao, *Polym. Chem.* **2012**, *3*, 343–351; c) B. V. K. J. Schmidt, T. Rudolph, M. Hetzer, H. Ritter, F. H. Schacher, C. Barner-Kowollik, *Polym. Chem.* **2012**, *3*, 3139–3145.
- [9] a) *Biochemistry and Binding: Activation of Small Molecules* (Eds.: K. M. Kadish, K. M. Smith, R. Guilard), Vol. 4, Academic Press, San Diego, **2000**; b) *Applications: Past, Present and Future* (Eds.: K. M. Kadish, K. M. Smith, R. Guilard), Vol. 6, Academic Press, San Diego, **2000**; c) J. R. Reimers, N. S. Hush, M. J. Crossley, *J. Porphyrins Phthalocyanines* **2002**, *6*, 795–805.
- [10] a) J. K. M. Sanders, N. Bampos, Z. Clyde-Watson, S. L. Darling, J. C. Hawley, H.-J. Kim, C. C. Mak, S. J. Webb, in *Axial Coordination Chemistry of Metalloporphyrins* (Eds.: K. M. Kadish, K. M. Smith, R. Guilard), Vol. 3, Academic Press, San Diego, **2000**; b) E. Alessio, I. Bouamaied, T. Coskun, G. Ercolani, L. Flamigni, M. J. Gunter, V. Heitz, J. T. Hupp, E. Iengo, Y. Kobuke, J.-P. Sauvage, F. Scandola, E. Stulz, *Non-Covalent Multi-Porphyrin Assemblies, Synthesis and Properties*, Springer, Berlin, **2006**; c) J. A. A. W. Elemans, R. van Hameren, R. J. M. Nolte, A. E. Rowan, *Adv. Mater.* **2006**, *18*, 1251–1266; d) J. L. Sessler, E. Karnas, E. Sedenberg, in *Porphyrins and Expanded Porphyrins as Receptors*, Wiley, **2012**.
- [11] a) R.-H. Jin, S. Aoki, K. Shima, *Chem. Commun.* **1996**, 1939–1940; b) R.-H. Jin, *Adv. Mater.* **2002**, *14*, 889–892; c) F. de Loos, I. C. Reinhout, J. Cornelissen, A. E. Rowan, R. J. M. Nolte, *Chem. Commun.* **2005**, 60–62; d) S. I. Yusa, T. Endo, M. Ito, *J. Polym. Sci. A Polym. Chem.* **2009**, *47*, 6827–6838; e) L. Wu, R. McHale, G. Q. Feng, X. S. Wang, *Int. J. Polymer Sci.* **2011**, 109693; f) T. Ren, A. Wang, W. Yuan, L. Li, Y. Feng, *J. Polym. Sci. A Polym. Chem.* **2011**, *49*, 2303–2313; g) C.-Y. Hsu, M.-P. Nieh, P.-S. Lai, *Chem. Commun.* **2012**, *48*, 9343–9345.
- [12] P. A. J. de Witte, M. Castriciano, J. Cornelissen, L. M. Scolaro, R. J. M. Nolte, A. E. Rowan, *Chem. Eur. J.* **2003**, *9*, 1775–1781.
- [13] M. M. Unterlass, E. Espinosa, F. Boisson, F. D'Agosto, C. Boisson, K. Ariga, I. Khalakhan, R. Charvet, J. P. Hill, *Chem. Commun.* **2011**, *47*, 7057–7059.
- [14] Y. Kim, M. F. Mayer, S. C. Zimmerman, *Angew. Chem.* **2003**, *115*, 1153–1158; *Angew. Chem. Int. Ed.* **2003**, *42*, 1121–1126.
- [15] a) V. V. Rostovtsev, L. G. Green, V. V. Fokin, K. B. Sharpless, *Angew. Chem.* **2002**, *114*, 2708–2711; *Angew. Chem. Int. Ed.* **2002**, *41*, 2596–2599; b) C. W. Tornøe, C. Christensen, M. Meldal, *J. Org. Chem.* **2002**, *67*, 3057–3064.
- [16] a) J. Chiefari, Y. K. Chong, F. Ercole, J. Krstina, J. Jeffery, T. P. T. Le, R. T. A. Mayadunne, G. F. Meijs, C. L. Moad, G. Moad, E. Rizzardo, S. H. Thang, *Macromolecules* **1998**, *31*, 5559–5562; b) S. Perrier, P. Takolpuckdee, *J. Polym. Sci. A Polym. Chem.* **2005**, *43*, 5347–5393; c) C. Barner-Kowollik, S. Perrier, *J. Polym. Sci. A Polym. Chem.* **2008**, *46*, 5715–5723; d) G. Moad, E. Rizzardo, S. H. Thang, *Aust. J. Chem.* **2009**, *62*, 1402–1472; e) M. Semsarilar, S. Perrier, *Nat. Chem.* **2010**, *2*, 811–820.
- [17] a) B. C. Bookser, T. C. Bruce, *J. Am. Chem. Soc.* **1991**, *113*, 4208–4218; b) J. E. A. Webb, F. Maharaj, I. M. Blake, M. J. Crossley, *Synlett* **2008**, 2147–2149; c) L. Le Pleux, Y. Pellegrin, E. Blart, F. Odobel, A. Harriman, *J. Phys. Chem. A* **2011**, *115*, 5069–5080.
- [18] D. Konkolewicz, A. Gray-Weale, S. Perrier, *J. Am. Chem. Soc.* **2009**, *131*, 18075–18077.
- [19] a) R. Chapman, K. A. Jolliffe, S. Perrier, *Aust. J. Chem.* **2010**, *63*, 1169–1172; b) R. Chapman, K. A. Jolliffe, S. Perrier, *Polym. Chem.* **2011**, *2*, 1956–1963; c) C. K. Poon, R. Chapman, K. A. Jolliffe, S. Perrier, *Polym. Chem.* **2012**, *3*, 1820–1826.

- [20] The method for calculating the reaction conversion by ^1H NMR is described in the Supporting Information, Section S4.
- [21] A. Sikorski, P. Romiszowski, *J. Chem. Phys.* **1998**, *109*, 6169–6174.
- [22] N. Fazeli, N. Mohammadi, F. A. Taromi, *Polym. Test.* **2004**, *23*, 431–435.
- [23] The two-arm model compound, $(\text{TA})_2\text{-Zn}$ was unsuitable for self-assembly studies due to its extremely low solubility in chloroform and other non-coordinating solvents. Its greatly improved solubility in pyridine suggests that zinc-triazole coordination contributes to its low solubility.
- [24] a) M. Kimura, Y. Nakano, N. Adachi, Y. Tatewaki, H. Shirai, N. Kobayashi, *Chem. Eur. J.* **2009**, *15*, 2617–2624; b) A. Eggenspieler, A. Takai, M. E. El-Khouly, K. Ohkubo, C. P. Gros, C. Bernhard, C. Goze, F. Denat, J.-M. Barbe, S. Fukuzumi, *J. Phys. Chem. A* **2012**, *116*, 3889–3898.
- [25] R. T. Stibrany, J. Vasudevan, S. Knapp, J. A. Potenza, T. Emge, H. J. Schugar, *J. Am. Chem. Soc.* **1996**, *118*, 3980–3981.
- [26] R. J. Abraham, S. C. M. Fell, H. Pearson, K. M. Smith, *Tetrahedron* **1979**, *35*, 1759–1766.
- [27] R. J. Abraham, K. M. Smith, *J. Am. Chem. Soc.* **1983**, *105*, 5734–5741.
- [28] K. J. Cross, M. J. Crossley, *Aust. J. Chem.* **1992**, *45*, 991–1004.
- [29] a) J. C. Hawley, N. Bampos, R. J. Abraham, J. K. M. Sanders, *Chem. Commun.* **1998**, 661–662; b) Y. Tong, D. G. Hamilton, J. C. Meillon, J. K. M. Sanders, *Org. Lett.* **1999**, *1*, 1343–1346; c) H. J. Kim, N. Bampos, J. K. M. Sanders, *J. Am. Chem. Soc.* **1999**, *121*, 8120–8121; d) J. C. Hawley, N. Bampos, J. K. M. Sanders, *Chem. Eur. J.* **2003**, *9*, 5211–5222.
- [30] Y. Kobuke, H. Miyaji, *J. Am. Chem. Soc.* **1994**, *116*, 4111–4112.
- [31] A. Satake, Y. Kobuke, *Org. Biomol. Chem.* **2007**, *5*, 1679–1691.
- [32] C. Maeda, S. Yamaguchi, C. Ikeda, H. Shinokubo, A. Osuka, *Org. Lett.* **2008**, *10*, 549–552.
- [33] K. Ding, F. Wang, F. Wu, *J. Photochem. Photobiol. A* **2011**, *220*, 64–69.
- [34] M. Pons, O. Millet, *Prog. Nucl. Magn. Reson. Spectrosc.* **2001**, *38*, 267–324.
- [35] S. Zaitzeva, S. Zdanovich, T. Ageeva, A. Ocheretovi, O. Golubchikov, *Molecules* **2000**, *5*, 786–796.
- [36] C.-H. Lee, S. Lee, H. Yoon, W.-D. Jang, *Chem. Eur. J.* **2011**, *17*, 13898–13903.
- [37] C. Hunter, H. Anderson, *Angew. Chem.* **2009**, *121*, 7624–7636; *Angew. Chem. Int. Ed.* **2009**, *48*, 7488–7499.
- [38] P. Klán, J. Wirz, *Photochemistry of organic compounds*, Wiley, Chichester, **2009**.
- [39] Multiple peak-fitting analysis was performed using Wavemetrics IgorPro data analysis software. See Supporting Information, Section S5 for details.
- [40] The self-assembly model is derived in full in the Supporting Information (Section S11).
- [41] M. M. J. Smulders, M. M. L. Nieuwenhuizen, T. F. A. de Greef, P. van der Schoot, A. Schenning, E. W. Meijer, *Chem. Eur. J.* **2010**, *16*, 362–367.
- [42] C. H. Kirksey, P. Hambright, C. B. Storm, *Inorg. Chem.* **1969**, *8*, 2141–2144.
- [43] A. Satake, Y. Kobuke, *Tetrahedron* **2005**, *61*, 13–41.
- [44] S. Hecht, H. Ihre, J. M. J. Frechet, *J. Am. Chem. Soc.* **1999**, *121*, 9239–9240.
- [45] W. R. Dichtel, K. Y. Baek, J. M. J. Fréchet, I. B. Rietveld, S. A. Vinogradov, *J. Polym. Sci. A Polym. Chem.* **2006**, *44*, 4939–4951.
- [46] W. L. F. Armarego, C. L. L. Chai, *Purification of Laboratory Chemicals*, Butterworth-Heinemann, Burlington, MA, 5th ed., **2003**.

Received: March 25, 2013

Published online: ■ ■ ■, 0000



Tunable building blocks: Triazole-linked porphyrin–polymer conjugates (PPCs) were prepared in high yield using the copper(I)-catalysed azide–alkyne cycloaddition (CuAAC) “click” reaction. The triazole groups were introduced from CuAAC coupling to guide the self-assembly of the PPCs into short oligomers (2–6 units in

length) via intermolecular porphyrinatozinc–triazole coordination. Association constants of the PPCs could be tuned by altering the polymer micro-environment around the porphyrin core, thus presenting a modular platform for designing self-assembled porphyrin–polymer materials.

Porphyrins

*D. A. Roberts, T. W. Schmidt,
M. J. Crossley,* S. Perrier** ■■■■–■■■■

Tunable Self-Assembly of Triazole-Linked Porphyrin–Polymer Conjugates 